A Neural Mechanism for Microsaccade Generation in the Primate Superior Colliculus

Ziad M. Hafed,[1]* Laurent Goffart,[2] Richard J. Krauzlis[1]

During fixation, the eyes are not still but often exhibit microsaccadic movements. The function of microsaccades is controversial, largely because the neural mechanisms responsible for their generation are unknown. Here, we show that the superior colliculus (SC), a retinotopically organized structure involved in voluntary-saccade target selection, plays a causal role in microsaccade generation. Neurons in the foveal portion of the SC increase their activity before and during microsaccades with sizes of only a few minutes of arc and exhibit selectivity for the direction and amplitude of these movements. Reversible inactivation of these neurons significantly reduces microsaccade rate without otherwise compromising fixation. These results, coupled with computational modeling of SC activity, demonstrate that microsaccades are controlled by the SC and explain the link between microsaccades and visual attention.

Microsaccades are the very small (typically <12 min arc), involuntary, fast eye movements that occur during fixation (*1*–*3*). The behavioral properties and functional role of microsaccades have been extensively studied, and sometimes vigorously debated, for many years (*1*–*14*). However, the neural mechanisms responsible for their generation are unexplored. We show that the superior colliculus (SC), a retinotopically organized structure known to be important for selecting and initiating voluntary eye movements (*15*–*17*), is also part of the neural mechanism that controls microsaccades.

We analyzed SC activity associated with 15,205 microsaccades that occurred while monkeys fixated a small stationary spot (*18*). Each fixation trial lasted for 3500 ms, resulting in many microsaccades with a variety of directions and amplitudes (Fig. 1A and fig. S1). These movements had dynamics like those of larger saccades (*3*) (fig. S1A), consistent with evidence that premotor neurons (downstream from the SC) are active during movements as small as 12 to 15 min arc (*19*).

We targeted neurons in the rostral pole of the SC, which represents foveal goal locations (*18*, *20*). Figure 1A shows the spiking activity of a neuron in the left SC during a single trial containing nine microsaccades (highlighted in green). The neuron exhibited changes in activity that were correlated with microsaccades. For example, the microsaccades labeled 1 and 2 in Fig. 1A were predominantly downward and leftward, respectively, and both were associated with a reduction in the neuron's activity. In contrast, small, predominantly rightward microsaccades, such as the ones labeled 3 and 4, caused an increase in activity before microsaccade onset and

[1]Systems Neurobiology Laboratory, Salk Institute for Biological Studies, 10010 North Torrey Pines Road, La Jolla, CA 92037, USA. [2]Institut de Neurosciences Cognitives de la Méditerranée, Equipe Dynamique de la Perception Visuelle et de l'Action, UMR 6193, CNRS–Aix-Marseille Universités, 13402 Marseille, France.

*To whom correspondence should be addressed. E-mail: zhafed@salk.edu

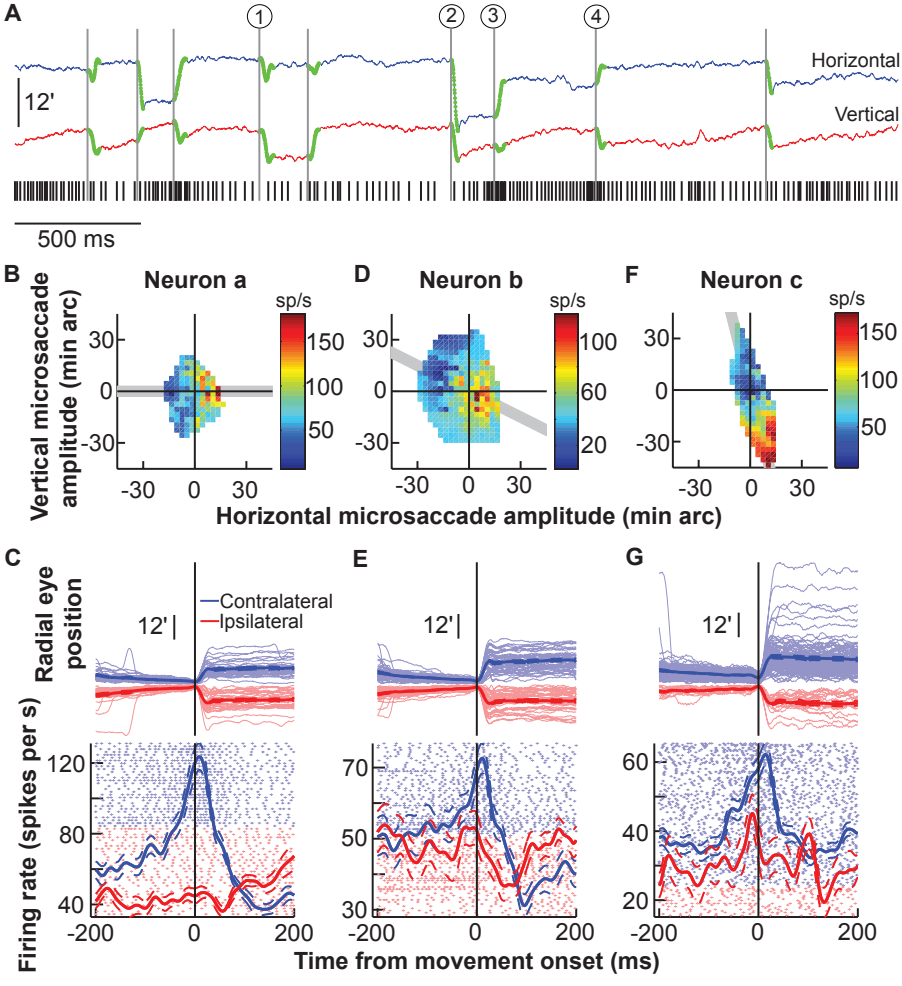

Fig. 1. Microsaccade-related activity in the SC. (**A**) Sample trial from one neuron. Microsaccades are highlighted in green on the eye position traces (*18*); the black tick marks indicate the neuron's spike times. The circled numbers highlight sample microsaccades that were associated with either a reduction in the neuron's activity (1 and 2) or a gradual build-up until movement onset (3 and 4). Upward deflections in the eye position traces denote right or up. (**B**) Peak discharge of the same neuron during all microsaccades plotted as a function of their horizontal and vertical amplitudes. The neuron preferred rightward movements sp, spikes. (**C**) Radial eye positions and neuronal activity for all microsaccades in the shaded gray region of (B) for the same neuron. Data are aligned on microsaccade onset and sorted by radial amplitude for contralateral (light blue) and ipsilateral (light red) movements. The vertical starting positions for successive microsaccade traces are also aligned but slightly offset from each other (by 0.06 min arc each) to facilitate visualization. Blue and red show average eye position or firing rate (with SEM envelopes). Light-colored dots show individual-movement spike rasters. (**D** and **E**) Similar to (B) and (C) but for another neuron, recorded from the same SC side, which preferred smaller movements directed to the lower right quadrant. (**F** and **G**) Similar to (B) and (C) but for a third neuron, from the same SC side, preferring larger movements (*22*).

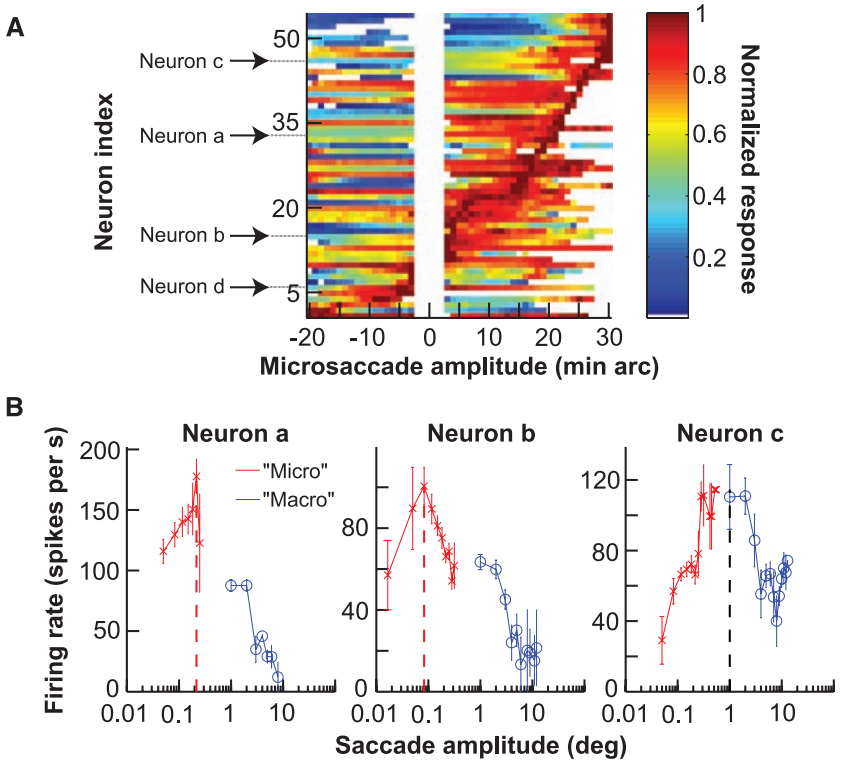

Fig. 2. Continuum of SC activity down to the smallest detectable saccades. (**A**) Peak discharge of each neuron during microsaccades plotted as a function of microsaccade amplitude along the neuron's preferred direction (positive is contralateral). Neurons are sorted on the basis of the amplitude that caused peak activity. Labeled neurons are the sample neurons of Fig. 1 and fig. S2 (for neuron d). White space in middle indicates unanalyzed bins (*18*). Each shown bin contains at least five microsaccades. (**B**) Comparison of neuronal activity during contralateral microsaccades along the neurons' preferred directions with activity during larger contralateral voluntary saccades. Some neurons were specifically tuned for microsaccades and paused or significantly reduced their activity for larger macrosaccades (neurons a and b). Other neurons continued to increase their discharge for slightly larger saccades (neuron c, fig. S3). Error bars denote SEM.

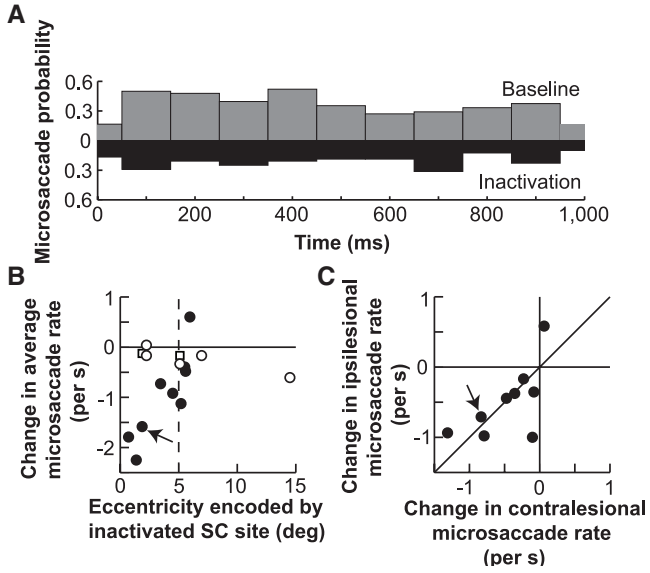

Fig. 3. A causal role for the SC in microsaccade generation. (**A**) Microsaccade probability during 1 s of fixation before (gray) and after (black) SC inactivation in one experiment [from monkey A (*18*)]. Inactivation reduced microsaccade rate. (**B**) Change in average microsaccade rate as a result of SC inactivation (average inactivation rate minus average baseline rate). Inactivation of the most central (i.e., rostral) SC sites caused the biggest reductions in microsaccades. Solid symbols indicate changes with $P < 0.05$ (rank-sum test, $N = 48$ trials for baseline, $N = 48$ trials for inactivation; average P value across solid symbols = 0.018). Squares indicate saline controls, which did not influence microsaccade rate. For a plot of absolute microsaccade rates before and after inactivation (also separated by monkey), see fig. S7. (**C**) Inactivation reduced both contralesional and ipsilesional microsaccades. For the experiments with a significant change in (B) ($N = 9/14$ experiments), data are plotted separately for contralesional and ipsilesional microsaccades. Eight of nine experiments fell in the lower left quadrant. Arrows in (B) and (C) point to the sample experiment of (A), performed at the same SC site as a subsequent saline control [square at the same eccentricity in (B)].

a burst during the movement itself. Thus, the neuron preferred particular microsaccade directions and amplitudes. We characterized these preferences across all microsaccades by plotting the neuron's activity as a function of the two-dimensional microsaccade amplitude, and we found consistent increases in activity for predominantly rightward microsaccades (Fig. 1B, neuron a). We also inspected the time course of the neuron's microsaccade-related activity. For this analysis, we included only microsaccades along the neuron's preferred axis (shaded region in Fig. 1B) to highlight activity associated with the preferred and nonpreferred directions, and we sorted the movements by radial amplitude to facilitate visualization (Fig. 1C). The neuron's activity was remarkably similar to the stereotypical saccade-related activity observed in caudal "build-up" neurons (*21*) during large "macro" saccades (see fig. S4, top, for samples), except that it happened for the smallest detectable eye movements.

Each neuron from the rostral SC exhibited individual preferences for a range of microsaccade directions and amplitudes. Figure 1, D to G, shows the activity of two additional sample neurons (neurons b and c), again recorded from the left SC, that preferred movements to the lower right quadrant. Neuron b showed a peak in discharge for ~6–min arc amplitudes and reduced its activity for smaller and larger movements. Thus, neuron b was tuned for saccade amplitudes smaller than those preferred by neuron a and also increased its activity for small leftward (i.e., ipsilateral) movements (Fig. 1D). Neuron c was tuned for amplitudes larger than those preferred by neuron a and increased its discharge for progressively larger microsaccades, up to ~44 min arc (Fig. 1F) (*22*).

Data from our population of neurons indicated that the SC contains a continuous representation of saccade amplitude and direction down to the smallest eye movements. We measured the activity of each neuron as a function of microsaccade amplitude along its preferred direction and sorted the neurons on the basis of their preferred microsaccade amplitudes (Fig. 2A). Neurons tiled the contralateral space of all measured microsaccade amplitudes and included some neurons whose activity was highest for ipsilateral movements as well. The raw activity of one of these neurons preferring ipsilateral microsaccades (labeled neuron d in Fig. 2A) is shown in fig. S2. The presence of such activity indicates that microsaccades involve activity distributed across the two SCs, functionally bridging the two visual hemi-fields to represent central targets.

Consistent with a continuous spatial representation throughout the SC (*21*), neuronal activity during microsaccades sometimes extended to small, voluntary saccades. Figure 2B illustrates this for the three sample neurons of Fig. 1 by plotting their activity as a function of amplitude during microsaccades, as well as during larger, visually guided saccades. This figure uses a logarithmic x-axis scale to magnify the representation of small microsaccades for easier visualization. Neurons a and b in Fig. 1 were specifically

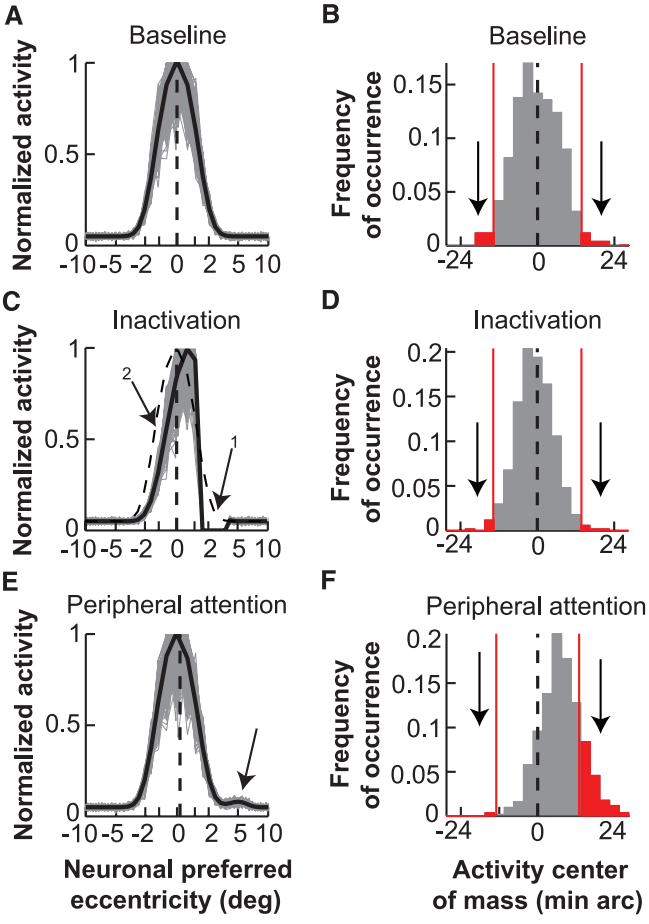

Fig. 4. A model of goal representation by the SC accounts for microsaccade generation. (**A**) Bilateral, one-dimensional SC map with activity representing the fixated goal. Activity is centered on neurons representing the central visual field (dashed black line). Gray traces show activity from 500 iterations of the model with each SC "neuron" exhibiting normally distributed activity (*18*). Negative values correspond to left, positive to right. (**B**) The instantaneous center of mass of SC activity in (A) was variable but had zero mean. Saccades are triggered when this center of mass deviates beyond a certain threshold (for example, red lines indicating 2 SD). (**C**) Simulating the effect of inactivating neurons representing ~2.5° (arrow 1). In the steady state, inactivation reduced the overall level of SC activity even on the intact side (arrow 2), but activity remained balanced bilaterally (vertical dashed line) (*24*). The dashed activity profile shows baseline. (**D**) The distribution of SC activity center of mass was narrower than in (B) but still had zero mean, explaining the reduction in both contralesional and ipsilesional microsaccades. For this simulation, there was a ~50% reduction in the frequency of deviations beyond the threshold of (B) (consistent with our experiments; fig. S7). (**E** and **F**) Simulating the momentary effects of a covert attention shift to a peripheral site at ~5° by introducing an increase in activity at this site (*18*). The average locus of activity was biased toward the peripheral site [dashed line in (E)], resulting in a higher probability of deviations from fixation toward the peripheral site than away from it (F).

tuned for movements with amplitudes classically associated with microsaccades, but neuron c was active for amplitudes that also included some voluntary movements larger than microsaccades. Similar observations were made for the remainder of our population. Neurons active during both microsaccades and voluntary saccades generally preferred voluntary saccades less than ~5° in amplitude (fig. S3). Neurons more caudal in the SC map (those preferring ~10° voluntary saccades in our data set) did not exhibit microsaccade-related activity (fig. S4).

SC activity during microsaccades was also distinct from modulations caused by small deviations of eye position from the fixated goal (*23*) (fig. S5), and it persisted in the absence of a visual stimulus (fig. S6).

We next investigated whether the SC is causally involved in microsaccade generation. Figure 3A shows the distribution of microsaccade occurrences during 1 s of steady-state fixation before and after reversibly inactivating a sample SC site. Inactivation caused a reduction in microsaccade rate (P = 0.0003; rank-sum test), and this was consistent across sessions, except when the inactivated SC neurons represented eccentricities larger than ~5° to 6° (Fig. 3B). This is consistent with our neuronal recordings that show a lack of microsaccade-related modulations for peripheral SC neurons (fig. S4). Inactivation reduced the probability of both contralesional and ipsilesional microsaccades (Fig. 3C), again consistent with our neuronal data showing activity for both contralateral and ipsilateral movements. Thus, rostral SC activity is directly involved in microsaccade generation.

A computational model, in which build-up neurons in the rostral SC encode foveal goal locations (*20*, *24*), provides a plausible mechanism for microsaccade generation (Fig. 4A). During steady-state fixation, the selected goal is foveal and results in bilateral activity centered on neurons representing the central visual field. The instantaneous locus of this activity may be viewed as a stochastic process with zero mean (Fig. 4B). According to this model, microsaccades are triggered when the center of mass of SC activity deviates sufficiently from zero.

Our model explains the inactivation-induced reduction in microsaccades. We simulated the effects of inactivation by eliminating the activity of a subset of model neurons (Fig. 4C, arrow 1). In steady state, inactivation reduces activity even on the intact side of the SC, without creating an imbalance across the right and left SC (*24*) (Fig. 4C). Thus, with the same stochastic processes influencing SC activity, the locus of the center of mass of this activity is less variable, which reduces the probability of deviation beyond the threshold for triggering saccades (Fig. 4D). Because the activity remains balanced bilaterally (*24*) (Fig. 4, C and D), inactivation reduces the frequency of both contralesional and ipsilesional microsaccades.

Our model can also explain why microsaccades are influenced by covert attention shifts (*8*, *9*). Cognitive factors such as attention and prior expectations alter build-up neuron activity (*25*, *26*); these changes could bias SC activity sufficiently to cause asymmetries in microsaccade generation. We therefore simulated the momentary effects on SC activity of attending to a peripheral location (Fig. 4E). These effects caused the average locus of SC activity to shift slightly toward the peripheral site, resulting in a higher probability of supra-threshold deviations toward the attended location (Fig. 4F).

Our results provide a description of the neural mechanisms for generating saccades smaller than 12 min arc. Coupled with the report that premotor neurons in the brainstem reticular formation are active during saccades as small as 12 to 15 min arc (*19*), our results demonstrate that microsaccades share the same neural mechanisms as voluntary saccades. Our proposal that microsaccade occurrence depends on the variability of SC activity representing salient goal locations reconciles seemingly disparate observations about microsaccades. Because SC activity can be manipulated by task set as well as by shifts of attention (*25*, *26*), this interpretation can explain why microsaccades might be voluntarily suppressed in some conditions (*6*) but asymmetrically increased in others (*8*, *9*) (Fig. 4F). Our interpretation also suggests that microsaccades may be part of a visual feedback loop. If the variability in target-related activity increases because of perceptual fading (*12*), the resulting microsaccades would correct for this fading through their influence on visual cortical activity (*27*–*30*). This in turn reduces the variability of SC signals defining the fixated target location. This mechanism can explain the increases in microsaccade rate and variability during fixation with no visual stimuli (*6*, *10*), as well as the behavioral correlations between increases or decreases in microsaccade rates and intensifying or fading visual percepts (*12*).

References and Notes

1. H. B. Barlow, *J. Physiol.* **116**, 290 (1952).
2. R. M. Steinman, G. M. Haddad, A. A. Skavenski, D. Wyman, *Science* **181**, 810 (1973).
3. B. L. Zuber, L. Stark, G. Cook, *Science* **150**, 1459 (1965).

4. B. Bridgeman, J. Palca, *Vision Res.* **20**, 813 (1980).
5. A. Kingstone, R. Fendrich, C. M. Wessinger, P. A. Reuter-Lorenz, *Percept. Psychophys.* **57**, 796 (1995).
6. R. M. Steinman, R. J. Cunitz, G. T. Timberlake, M. Herman, *Science* **155**, 1577 (1967).
7. B. J. Winterson, H. Collewijn, *Vision Res.* **16**, 1387 (1976).
8. Z. M. Hafed, J. J. Clark, *Vision Res.* **42**, 2533 (2002).
9. R. Engbert, R. Kliegl, *Vision Res.* **43**, 1035 (2003).
10. T. N. Cornsweet, *J. Opt. Soc. Am.* **46**, 987 (1956).
11. E. Kowler, R. M. Steinman, *Vision Res.* **20**, 273 (1980).
12. S. Martinez-Conde, S. L. Macknik, X. G. Troncoso, T. A. Dyar, *Neuron* **49**, 297 (2006).
13. F. Ratliff, L. A. Riggs, *J. Exp. Psychol.* **40**, 687 (1950).
14. S. Martinez-Conde, S. L. Macknik, D. H. Hubel, *Nat. Rev. Neurosci.* **5**, 229 (2004).
15. R. M. McPeek, E. L. Keller, *Nat. Neurosci.* **7**, 757 (2004).
16. C. D. Carello, R. J. Krauzlis, *Neuron* **43**, 575 (2004).
17. R. J. Krauzlis, *J. Neurosci.* **23**, 4333 (2003).
18. Materials and methods, including behavioral tasks, single-neuron recordings, and inactivations, are available as supporting material on *Science* Online.
19. J. A. M. Van Gisbergen, D. A. Robinson, S. A. Gielen, *J. Neurophysiol.* **45**, 417 (1981).
20. Z. M. Hafed, R. J. Krauzlis, *J. Neurosci.* **28**, 9426 (2008).
21. D. P. Munoz, R. H. Wurtz, *J. Neurophysiol.* **73**, 2313 (1995).
22. Because microsaccades are not under full experimental control, they posed special challenges, described in more detail in (*18*).
23. R. J. Krauzlis, M. A. Basso, R. H. Wurtz, *J. Neurophysiol.* **84**, 876 (2000).
24. Z. M. Hafed, L. Goffart, R. J. Krauzlis, *J. Neurosci.* **28**, 8124 (2008).
25. A. Ignashchenkova, P. W. Dicke, T. Haarmeier, P. Thier, *Nat. Neurosci.* **7**, 56 (2004).
26. M. A. Basso, R. H. Wurtz, *J. Neurosci.* **18**, 7519 (1998).
27. S. Martinez-Conde, S. L. Macknik, D. H. Hubel, *Nat. Neurosci.* **3**, 251 (2000).
28. D. A. Leopold, N. K. Logothetis, *Exp. Brain Res.* **123**, 341 (1998).
29. D. M. Snodderly, I. Kagan, M. Gur, *Vis. Neurosci.* **18**, 259 (2001).
30. W. Bair, L. P. O'Keefe, *Vis. Neurosci.* **15**, 779 (1998).
31. Funding provided by NIH grant EY12212 and Agence Nationale de la Recherche grant RETINAE. We thank K. Nielsen and V. Ciaramitaro for helpful comments.

Supporting Online Material
www.sciencemag.org/cgi/content/full/323/5916/940/DC1
Materials and Methods
Figs. S1 to S7

18 September 2008; accepted 10 December 2008
10.1126/science.1166112

An ABC Transporter Controls Export of a *Drosophila* Germ Cell Attractant

Sara Ricardo and Ruth Lehmann*

Directed cell migration, which is critical for embryonic development, leukocyte trafficking, and cell metastasis, depends on chemoattraction. 3-hydroxy-3-methylglutaryl coenzyme A reductase regulates the production of an attractant for *Drosophila* germ cells that may itself be geranylated. Chemoattractants are commonly secreted through a classical, signal peptide–dependent pathway, but a geranyl-modified attractant would require an alternative pathway. In budding yeast, pheromones produced by a-cells are farnesylated and secreted in a signal peptide–independent manner, requiring the adenosine triphosphate–binding cassette (ABC) transporter Ste6p. Here we show that *Drosophila* germ cell migration uses a similar pathway, demonstrating that invertebrate germ cells, like yeast cells, are attracted to lipid-modified peptides. Components of this unconventional export pathway are highly conserved, suggesting that this pathway may control the production of similarly modified chemoattractants in organisms ranging from yeast to humans.

In most organisms, primordial germ cells migrate from their site of origin to the somatic part of the gonad, where they develop into mature eggs and sperm. In *Drosophila*, germ cells migrate as single cells in a stereotyped manner and are guided by repellent and attractive cues toward the somatic gonad in the mesoderm (*1*). 3-hydroxyl-3-methyl-glutaryl-CoA reductase (HMG-CoAr or HMGCR) activity controls germ cell attraction to the mesoderm and the recruitment of germ cells to the somatic gonad. In *hmgcr* mutant embryos, germ cells fail to reach the somatic gonad; moreover, ectopic HMGCR expression is sufficient to attract germ cells to a new location (*2*). Embryos mutant for several enzymes in the *hmgcr* pathway, including the β subunit of type I geranygeranyl transferase (βGGTI), are similarly defective in germ cell migration, suggesting that geranylation is critical in attracting germ cells to the mesoderm (*3*).

Because *hmgcr* or *βggtI* mutant embryos show a rather specific germ cell migration defect, we favored the idea that the HMGCR pathway was required to geranylate a critical germ cell attractant rather than regulating a pathway that controlled synthesis or secretion of the attractant (*3*). This idea posits secretion of a geranyl-modified germ cell attractant, which would preclude secretion by a classic, signal peptide–dependent secretory pathway and require an alternative export mechanism. Such a mechanism has been described in yeast, where adenosine triphosphate (ATP)–binding cassette (ABC) transporters export farnesylated pheromones required for cell mating (*4*, *5*). We therefore asked whether a similar export mechanism exists in *Drosophila* and is required for germ cell attraction.

ABC transporters are conserved in organisms ranging from bacteria to humans and shuttle hydrophobic lipophilic compounds in an ATP-dependent manner (*6*, *7*). In *Saccharomyces cerevisiae* and *Schizosaccharomyces pombe*, the ABCB family members Ste6p and Mam1 play essential roles in the export of farnesyl-modified a-type and M-type mating factors, respectively. The human ABCB family member *mdr1* (*multidrug resistance*) gene is amplified in multidrug-resistant cells, and its homolog *mdr3* is a functional homolog of *STE6* (*8*, *9*), suggesting a close relationship between the ability of this class of transporters to export drugs and lipid-modified signaling molecules. To determine whether ABCB transporters have a role in exporting the putative *Drosophila* germ cell attractant, we analyzed expression patterns and germ cell migration in embryos mutant for ABCB transporters (*7*) (table S1). Among these, only *mdr49* showed an expression pattern and mutant phenotype consistent with a role in germ cell migration (Fig. 1A, fig. S1, and table S2). We generated a strong loss-of-function allele, $mdr49^{\Delta 3.16}$ (Fig. 1B, fig. S1A, and table S2), and $mdr49^{\Delta 3.16}$ mutant embryos showed defects in germ cell migration, like embryos in which the HMGCR pathway was mutant: Germ cells migrated through the posterior midgut but then failed to associate with the somatic gonad (Fig. 1C), which was properly specified (fig. S1E). This migration phenotype was observed only in *mdr49* mutants and not in mutants for other ABCB transporters, such as Mdr50, Mdr65, and CG7955 (table S1). To determine whether *mdr49* function is required in the mesoderm, we restored *mdr49* expression selectively in the mesoderm (fig. S1F) and found that it fully rescued the *mdr49* mutant phenotype (Fig. 1D). To test whether Mdr49 acts as an ABCB transporter, we asked whether Ste6p rescued the germ cell migration phenotype observed in *mdr49* embryos. Expressing *STE6* in the mesoderm rescued the migration defect (Fig. 1D and fig. S1F), suggesting that Mdr49 is functionally equivalent to Ste6p and acts in mesodermal cells to attract germ cells.

The germ cell migration phenotypes caused by mutations in Mdr49 and in components of the HMGCR pathway, such as geranylgeranyl-diphosphate synthase and ßGGTI, are strikingly similar (*2*, *3*). Thus, to determine whether Mdr49 acts as a transporter for a germ cell attractant that is geranylgeranyl-modified by the HMGCR pathway, we tested the genetic epistasis between *hmgcr* and *mdr49*. Previous experiments showed that overexpression of *hmgcr* in the central nervous system (CNS) is sufficient to attract germ cells to this tissue (*2*). We therefore reasoned that Mdr49 function should be necessary for the export of the ectopically produced attractant and that mutations in *mdr49* should suppress the *hmgcr* misexpression phenotype. Indeed, germ cell migration to the CNS was suppressed by reducing *mdr49* copy number by means of either the *mdr49* deficiency or P-element mutation. (Fig. 2 and table S3). Mutations in other ABCB transporters, such as *mdr50*, *mdr65*, and *CG7955*, did not significantly suppress the *hmgcr* overexpression pheno-

Howard Hughes Medical Institute (HHMI), Helen L. and Martin S. Kimmel Center for Biology and Medicine at the Skirball Institute, Department of Cell Biology, New York University School of Medicine, New York University, 540 First Avenue, New York, NY 10016, USA.

*To whom correspondence should be addressed. E-mail: lehmann@saturn.med.nyu.edu